



Cite this: *Phys. Chem. Chem. Phys.*,
2016, **18**, 17606

Insight into both coverage and surface structure dependent CO adsorption and activation on different Ni surfaces from DFT and atomistic thermodynamics†

Xiaobin Hao,^a Baojun Wang,^{*a} Qiang Wang,^b Riguang Zhang^{*a} and Debao Li^b

CO adsorption and activation on Ni(100), (110) and (111) surfaces have been systematically investigated to probe the effect of coverage and surface structure on CO adsorption and activation. Herein, dispersion-corrected density functional theory calculations (DFT-D) were employed, and the related thermodynamic energies at 523 K were calculated by including the zero-point energy, thermal energy and entropic corrections; the results show that the saturated coverage of CO on the Ni(111), (100) and (110) surfaces correspond to 8/9, 9/12 and 9/9 ML, respectively. As the coverage increases, the stepwise adsorption free energies decrease on the flat (111) and (100) surfaces, whereas small changes occur on the corrugated (110) surface. CO migrates from the three-fold hollow site to the top site on the (111) surface, and from the four-fold hollow to the two-fold bridge site on the (100) surface, while all the CO molecules remain at the short-bridge site on the (110) surface. As a result, the obtained intermolecular CO–CO repulsive interactions on the flat surface are stronger than the interactions on the corrugated surface. Furthermore, the computed CO vibrational frequencies at different levels of coverage over the Ni surfaces agree well with the experimental results. On the other hand, kinetic analyses were utilized to compare the stepwise CO desorption with the dissociation at different degrees of coverage on the three Ni surfaces. CO desorption is more favorable than its dissociation at all coverage levels on the most exposed Ni(111) surface. Analogously, CO desorption becomes more favorable than its dissociation on the Ni(110) surface at higher coverage, except for coverage of 1/9 ML, in which CO desorption competes with its dissociation. However, on the Ni(100) surface, CO dissociation is more favorable than its desorption at 1/12 ML; when the coverage increases from 2/12 to 3/12 ML, equilibrium states exist between dissociation and desorption over the surface; when the coverage is greater than or equal to 4/9 ML, CO desorption becomes more favorable than dissociation. By applying the atomistic thermodynamics method, the determination of stable coverage as a function of temperature and partial pressure provides useful information, not only for surface science studies under ultrahigh vacuum conditions, but also for practical applications at high temperature and pressure in exploring reactions.

Received 12th March 2016,
Accepted 18th May 2016

DOI: 10.1039/c6cp01689h

www.rsc.org/pccp

1 Introduction

Carbon monoxide (CO) is a very important basic chemical that has been widely used in many catalytic processes, such as the

carbon-one reactions, Fischer–Tropsch synthesis, water–gas reaction, car exhaust catalysis, and so on. These chemical processes have been carried out on the basis of heterogeneous catalysis,^{1,2} and the interactions between CO and metal surfaces

^a Key Laboratory of Coal Science and Technology of Ministry of Education and Shanxi Province, Taiyuan University of Technology, No. 79 Yingze West Street, Taiyuan 030024, Shanxi, P. R. China. E-mail: wangbaojun@tyut.edu.cn, zhangriguang@tyut.edu.cn; Fax: +86 351 6041237; Tel: +86 351 6018239

^b State Key Laboratory of Coal Conversion, Institute of Coal Chemistry, Chinese Academy of Sciences, Taiyuan 030001, Shanxi, P. R. China

† Electronic supplementary information (ESI) available: The thermodynamic correction expressions ΔE_{ads} (correction), ΔE_{a} (correction), and ΔE_{dis} (correction) have been given in Part 1. The stepwise CO adsorption energies at different coverage levels with and without dispersion correction have been presented in Table S1. The test results about the effect of vacuum thickness, supercell size and slab layers on CO adsorption energy over different Ni surface models have been presented in Table S2. The detailed presentations about the most stable adsorption configurations of CO, C and O atoms on Ni(111), (100) and (110) surfaces, and the initial and optimized structures, the total energies of adsorbed CO molecules at different coverage, as well as the structures of initial states, transition states and final states involved in the dissociations of CO molecules at different coverage on Ni surfaces have been presented in Fig. S1–S7. It is also noted that only the initial and optimized structures at the short-bridge site at different coverage levels on the Ni(110) surface are listed, since all CO molecules migrate from the other sites to the short-bridge site after geometry optimization. See DOI: 10.1039/c6cp01689h

play a key role in the initial step of these catalytic processes.^{3–8} CO adsorption and activation can affect the formation pathways of CH_x intermediates during the reactions related to syngas conversion.^{9,10} For example, when direct dissociation of CO into C is carried out, the CH_x intermediate is predominantly formed by C hydrogenation, whereas on CO hydrogenation to CH_xO or CH_xOH, followed by C–O bond cleavage, the CH_x intermediate is produced. Therefore, a preliminary understanding of CO adsorption and activation on the metal surfaces is necessary in order to probe the essential information for the initial step of these surface-catalyzed reactions.

Experimental studies on CO activation have thus far revealed that under realistic conditions, the catalyst surface is always covered by CO molecules.^{11,12} For example, Iglesia *et al.*³ have probed the effects of CO coverage on the binding energies and the C–O bond activation paths on Fe and Co catalysts, using experiments and theoretical calculations, which suggest that hydrogen-assisted CO activation is the predominant kinetically-relevant step. Compared to the adsorption energy of CO at the coverage of 0.25 ML on Fe and Co, at the coverage of 0.75 ML it decreases by about 1 eV on the respective surfaces. At high coverage on Ru catalyst,¹¹ the CO binding ability is reduced, and H-assisted dissociation is the predominant path for CO activation, instead of direct dissociation. Recently, using the DFT method, Jiao *et al.*^{12–15} also found that at high coverage on Fe and Mo₂C surfaces, the adsorption and dissociation of CO became more difficult. Furthermore, Scheijen *et al.*¹⁶ believe that the adsorption energies of CO are coverage-independent from 0.25 to 0.50 ML on the body-centered cubic metals. The above results therefore show that the effect of coverage on CO adsorption and activation is a key factor for the initial activation pathway of CO in the metal catalysis systems.

High activity and selectivity of Ni catalyst has been obtained in the methanation of syngas,^{17–20} in which CO adsorption and activation are the key initial steps of the methanation process. Among the three low-index surfaces of face-centered cubic Ni, the adsorption of CO on the close-packed Ni(111) surface has been widely studied in experiments. Using infrared reflection-absorption spectroscopy (IRAS), Greenler *et al.*²¹ and Surnev *et al.*²² have shown that CO molecules are adsorbed at the two-fold bridge and three-fold site under low coverage, and move from the three-fold to the two-fold bridge site with increasing coverage, which also agrees with the previous results.^{23–26} However, scanning tunneling microscope (STM) images have shown that CO occupies both fcc and hcp three-fold sites with the molecular axis tilted with respect to the surface normal.²⁷ Held *et al.*²⁸ reported that CO resides at the three-fold site for low coverage up to 0.50 ML, based on low energy electron diffraction (LEED) and X-ray photoelectron spectroscopy (XPS) and temperature programmed desorption (TPD) studies. Further, CO molecules occupy the same hollow sites at 0.50 ML coverage, as observed by photoelectron diffraction (PED),^{29,32} surface extended X-ray-absorption fine-structure studies (SEXAFS)³⁰ and LEED.³¹ In addition, CO prefers to desorb from the Ni surface, rather than dissociate at low coverage, as concluded by Ng *et al.*³³ and Andersson *et al.*³⁴

On the Ni(100) surface, Lauterbach *et al.*³⁵ reported that CO molecules are arranged in incommensurate or weakly incommensurate adsorbate layers above the coverage of 0.50 ML, and Biberian *et al.*³⁶ showed the different regular structures at coverage >0.50 ML, based on LEED, high resolution energy electron loss spectroscopy (EELS) and infrared spectroscopy (IRS). The variation of the occupation ratio of terminal to bridged CO species at the low coverage at 18 K strongly suggests that the substrate-mediated interactions between CO molecules operate at a relatively long range.³⁷ Subsequently, Rupprechter *et al.*³⁸ observed that CO adsorbs at the top site, but the bridge-bonded CO at the coverage ≤0.50 ML could not be detected using infrared-visible sum frequency generation (SFG) surface vibrational spectroscopy, which agrees with the previous work by Pendry *et al.*,³⁹ using LEED at 120 K.

On the Ni(110) surface, regarded as the most strongly corrugated of the low-index fcc surfaces, some studies such as LEED,^{40,43} SEXAFS⁴¹ and EELS,^{42,44} as well as high resolution IRS,⁴⁵ have suggested that CO prefers to adsorb at the short bridge site at high coverage. However, other studies involving LEED,⁴⁶ off-specular EELS⁴⁷ and X-ray photoelectron diffraction⁴⁸ (XRD), claim that CO favors the top site. Voigtländer *et al.*⁴⁷ attributed the difference to the fact that the previous specular EELS assignments to the short bridge site relied on an interpretation of a marginal excitation peak frequency.

As mentioned above, extensive experimental studies on Ni surfaces have investigated CO adsorption and activation; however, the preferable adsorption site of CO from low to high coverage on Ni surfaces remains controversial. Moreover, coverage dependent CO adsorption on Ni surfaces is not well addressed. Nowadays, theoretical investigations have provided useful information for understanding the adsorption configurations of CO molecules and its dissociation at different degrees of coverage over metal surfaces.^{12–15} For CO adsorption and dissociation on Ni surfaces, some theoretical studies have been carried out. For example, on the Ni(111) surface, DFT^{49–51} results have indicated that CO prefers to be adsorbed at the hcp site at the coverages of 0.33, 0.25 and 0.50 ML, and the barrier for CO dissociation are higher than its desorption energy at 0.25 ML^{52,56} and 0.11 ML.^{53–55} Hammer *et al.*⁵⁷ and Zhou *et al.*⁵⁸ have shown that CO prefers to adsorb at the hollow site, rather than the top and bridge sites on Ni(100) surfaces with coverage of 0.25 and 0.17 ML, respectively. Moreover, Andersson *et al.*³⁴ studied the activation pathways of CO at two different levels of coverage on the Ni(100) surface, and concluded that the COH route is more likely to occur than the direct dissociation. Demirci *et al.*⁵⁹ investigated CO adsorption at the top and short-bridge sites on the Ni(110) surface, with coverage of 0.25, 0.50, 0.75 and 1.00 ML. Mohsenzadeh *et al.*⁶⁰ suggested that the desorption and dissociation barriers of CO have little difference (1.89 vs. 1.83 eV) on the Ni(110) surface at the coverage of 0.25 ML.

On the basis of the importance of CO adsorption and activation on Ni surfaces, the reported theoretical studies have provided useful information for understanding CO adsorption and activation, and explained many experimental findings on a microscopic scale. However, some key factors should also be

considered: (a) coverage dependent CO adsorption and activation on Ni surfaces is not well addressed; (b) the effect of Ni surface structures on CO adsorption and activation has not been systematically mentioned; (c) the effect of temperature and CO partial pressure on CO surface coverage has not been considered. Therefore, in order to account for the above considerations, in this study, we have carried out the systematic DFT calculations, together with thermodynamic and kinetic models to investigate CO adsorption, dissociation, and desorption at different levels of coverage and different conditions on Ni(111), (100) and (110) surfaces.

2 Computational details

2.1 Calculation methods

All calculations have been performed using the periodic DFT with the projector-augmented wave (PAW) method that is implemented in the Vienna Ab Simulation Package (VASP).^{61,62} The exchange correlation energy of the electrons is treated with the generalized gradient approximation (GGA) in the Perdew–Burke–Ernzerhof (PBE) formalism,^{63,64} which is widely used in various systems, such as the Fe and Mo₂C system,^{12–15} as well as the Ni system.^{60,65,66} Moreover, considering the long-range dispersion corrections for van der Waals interactions, the DFT-D method is used in this study.^{67,68} Our results show that DFT and DFT-D calculations give negligible differences for the adsorption configurations and energies of the stepwise CO adsorption on Ni surfaces at different levels of coverage, with and without dispersion correction (see Table S1, ESI†). The reason may be that DFT-D methods well describe the weak physical adsorption and the conformations of long-chain alkane and molecular clusters. For example, Jordan *et al.*⁶⁹ have employed DFT-D calculations to correct the CO₂–surface interactions because CO₂ molecules interact relatively weakly with the rutile (110) surface. Chen *et al.*⁷⁰ have also employed DFT-D correction to investigate the conformation of (H₂)₂ and (N₂)₂ clusters.

Since Ni is a magnetic metal, spin-polarized calculations are applied to correctly account for its magnetic properties, which were found to be essential for an accurate description of adsorption energy.⁷¹ A cutoff energy of 400 eV was used for a plane-wave basis set, electronic convergence was set to 5×10^{-6} eV, and the forces converged to $0.03 \text{ eV } \text{Å}^{-1}$. A $3 \times 3 \times 1$ *k*-points grid was used for sampling the Brillouin zone, and the smearing width was 0.20 eV. The vibrational frequency for the adsorbed system was determined in single point calculations with the metal atoms fixed at their positions.⁷²

The bulk lattice constant and magnetic moment of Ni were calculated to be 3.524 Å and 1.63 μB per atom, which agree well with the experimental values of 3.523 Å⁷³ and 1.61 μB,⁷⁴ respectively. The gaseous CO molecule was optimized in a $10 \times 10 \times 10$ Å cubic cell with a single *k*-point.⁷⁵ The C–O bond length was calculated to be 1.144 Å, which is close to the experimental value of 1.130 Å.⁷⁶

On the other hand, in order to locate the transition states of CO dissociation on Ni surfaces, the climbing-image nudged

elastic band method (CI-NEB)^{77,78} was carried out to obtain minimum energy paths, which were decided with at least four optimized iteratively intermediate images between the initial and final states. The images of highest energy along the reaction coordinates were designated as the transition-state structures, and the located transition states were optimized using the dimer method,^{79,80} and were further confirmed by the existence of only one imaginary frequency. The forces for all atoms in the transition state structures were less than $0.05 \text{ eV } \text{Å}^{-1}$.

2.2 Surface model

In order to probe the complex CO equilibrium adsorption on all three low-index surfaces of Ni at different levels of coverage, before the calculations of CO adsorption and activation, we tested the effect of vacuum thickness (10 Å, 12 Å, 15 Å), the supercell size ($p(3 \times 3)$, $p(3 \times 4)$, $p(4 \times 4)$), and the slab layers (3, 4, 5 layers for Ni(111) and (100) surfaces, and 4, 5, 6 layers for Ni(110) surface) of different Ni surfaces on CO adsorption. The corresponding results are listed in Table S2 (ESI†).

According to the data in Table S2 (ESI†), the three low-index Ni surfaces maintained the vacuum of 10 Å between the repeated slabs to exclude the slab interactions. The Ni(111), (100) and (110) surfaces were modeled using the $p(3 \times 3)$, $p(3 \times 4)$ and $p(3 \times 3)$ unit cells, respectively. The slab thickness of four-layers was used to model the (111) and (100) surfaces, and a thickness of five-layers was used to model the (110) surface; these have been widely used in previous studies.^{52,54,81–85} In the model tests, the top two layers of atoms and all adsorbed species were allowed to relax, while the remaining layers were fixed in their bulk positions.

Fig. 1 presents the different adsorption sites on three low-index Ni surfaces. The (111) surface is the flat surface with four adsorption sites: top (T), bridge (B), hcp and fcc (three-fold hollow) sites. The (100) surface is also the flat surface, which has three adsorption sites: top (T), bridge (B) and four-fold hollow sites (4F). However, the (110) surface presents the corrugated surface, which has five adsorption sites: top (T),

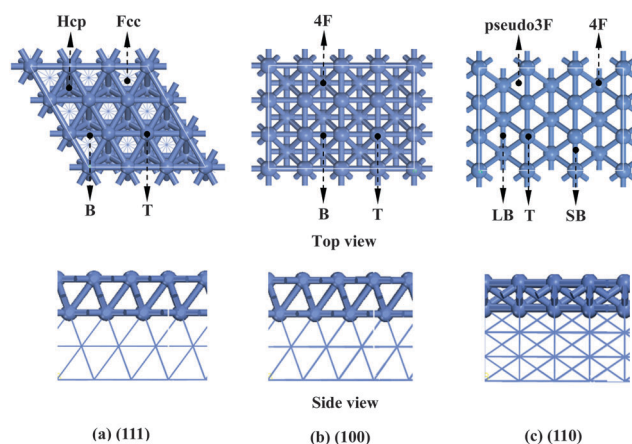


Fig. 1 The top and side views of the Ni(111), (100) and (110) surfaces, together with the different adsorption sites.

long-bridge (LB), short-bridge (SB), four-fold hollow (4F) site and the pseudo three-fold hollow site (pseudo 3F).

2.3 Thermodynamics

As mentioned in many previous studies,^{86–88} the methanation of syngas, catalyzed by Ni-based catalysts was carried out at a temperature around 523 K, at which higher activity and higher CO conversion were exhibited. Therefore, in order to provide deep analysis and practical applications of CO adsorption and activation at the different levels of coverage on the Ni surfaces, the Gibbs free energy^{89,90} at the temperature of 523 K is given in Sections 3.2–3.4 by the following eqn (1):

$$G^\theta(T, p) = E_{\text{total}} + E_{\text{ZPE}} + U^\theta - TS^\theta + \gamma RT [1 + \ln(p_{\text{CO}}/p^\theta)] \quad (1)$$

where E_{total} is the total energy determined by DFT calculations, E_{ZPE} is the zero-point vibrational energy, R is the gas constant, p_{CO} is the partial pressure of the gas-phase CO molecule.

As for the gaseous CO molecule, γ is equal to 1, the thermal change from 0 K to 523 K and the standard entropy at the temperature of 523 K can be calculated using the Shomate equation, and the related parameters are taken from ref. 76.

E_{ZPE} is the zero-point vibrational energy, which is calculated by the following eqn (2):

$$E_{\text{ZPE}} = \sum_{i=1}^n \frac{N_A h \nu_i}{2} \quad (2)$$

where h is Planck's constant, ν_i refers to vibrational frequency, and N_A is Avogadro's number.

As for the tightly bound species involved in CO, C and O adsorption at different levels of coverage, the translational and rotational modes were replaced by vibrational modes, and γ is equal to 0. Consequently, the standard molar thermal change and entropy of these adsorbed species are given by the eqn (3) and (4), where k_B is Boltzmann's constant.

$$U^\theta = \sum_{i=1}^n \frac{N_A h \nu_i}{e^{k_B T} - 1} \quad (3)$$

$$S^\theta = \sum_{i=1}^n \left[-R \ln \left(1 - e^{-\frac{h \nu_i}{k_B T}} \right) + \frac{N_A h \nu_i}{e^{k_B T} - 1} \frac{1}{T} \right] \quad (4)$$

On the other hand, the atomistic thermodynamics method has been employed as the key measure to connect the practical reaction conditions with the theoretical calculations. This method has been successfully applied in many systems.^{12–15} In this study, for the adsorption of $n\text{CO}$ molecules on the surface, the change in the Gibbs free energy at the given temperature and CO pressure is obtained using the following equations:

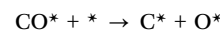
$$\Delta G(T, p, n_{\text{CO}}) = E_{\text{slab}/n_{\text{CO}}} - E_{\text{slab}} - [nE_{\text{CO}} + nG(T, p^\theta) + nk_B T \ln(p_{\text{CO}}/p^\theta)] \quad (5)$$

In this equation, $E_{\text{slab}/n_{\text{CO}}}$, E_{slab} and E_{CO} refer to the total energies of the slab surface with n adsorbed CO molecules, the corresponding bare slab surface, and the single CO

molecule obtained from DFT calculations, respectively. $G(T, p^\theta)$ was calculated by Gaussian software, considering the vibrational, translational and rotational contributions of the CO molecule in the gas phase, n is the number of the CO species, k_B is the Boltzmann constant, p^θ is the standard atmospheric pressure. The detailed descriptions of the method have been presented previously.^{12–15}

2.4 Kinetic model

In order to compare the stepwise CO desorption and dissociation at different levels of coverage on Ni metal, a simple kinetic model was used.



The CO dissociation rate is $r_{\text{dis}} = k_{\text{dis}} \theta_{\text{CO}^*} \theta^*$, while the desorption rate is $r_{\text{des}} = k_{\text{des}} \theta_{\text{CO}^*}$; θ_{CO^*} is the coverage of adsorbed CO, and θ^* is the coverage of the free sites. Both rate constants are derived from transition state theory (TST),⁹¹ given by the following eqn (6):

$$k = \frac{k_B T}{h} \left(\frac{p^\theta}{RT} \right)^{1-n} e^{-\frac{\Delta G^\ddagger, \theta}{RT}} \quad (6)$$

where, k is the rate constant, T is the reaction temperature, k_B , h , p^θ and R are Boltzmann's constant, Planck's constant, standard atmospheric pressure and the fundamental gas constant, respectively. n is the number of reactants, and $\Delta G^\ddagger, \theta$ is the change in the standard molar Gibbs free energy barrier, which is the activation barrier from DFT calculations with the thermodynamic correction.

3 Results and discussion

3.1 CO, C and O adsorption

The adsorption energy (E_{ads}) is always regarded as a measure of strength for the adsorbate–substrate interaction. The adsorption energy of the adsorbed species on the slab surface can be expressed as follows:

$$E_{\text{ads}} = E_{\text{s}/\text{slab}} - (E_{\text{slab}} + E_{\text{s}}) \quad (7)$$

where $E_{\text{s}/\text{slab}}$ is the total energy of the slab surface with the adsorbed species, E_{slab} is the total energy of the corresponding bare slab surface, E_{s} is the total energy of the gas-phase species. With this definition, the more negative E_{ads} is, the stronger the adsorption is. The most stable configurations of the single CO, C and O adsorptions on Ni(111), (100) and (110) surfaces are shown in Fig. S1 (ESI†).

3.1.1 Ni(111) surface. For the single CO molecule, our calculated results show that CO prefers to adsorb at the hcp site (−1.93 eV), then the fcc (−1.91 eV), bridge (−1.78 eV) and top (−1.49 eV) sites, which are in accordance with the previous results.^{49–51,92} The adsorption energy (−1.93 eV) at the hcp site is similar to that (−1.92 eV) obtained by Yuan *et al.*,⁵⁵ using the same surface size and functional. Moreover, the C–O bond

length at the hcp site is elongated to 1.195 Å, with the corresponding average Ni–C bond length of 1.947 Å.

For the adsorption of C and O atoms, no matter where the C or O atom is placed, they always migrate to the three-fold sites after geometry optimization, in which the C atom prefers the hcp site, while the O atom favors the fcc site. The adsorption energies of C and O atoms are –6.87 and –5.80 eV, respectively, the average C–Ni and O–Ni bond lengths are 1.768 and 1.843 Å, respectively, which are in good agreement with the previous DFT results.^{57,58}

3.1.2 Ni(100) surface. For one CO molecule, adsorption at the four-fold hollow site is the most stable configuration. The adsorption energy (–2.01 eV) is larger than the energy at the bridge and top sites, by 0.11 and 0.31 eV, respectively. The adsorption energy (–2.01 eV) at the four-fold hollow site is similar to that obtained by Hammer *et al.* (–2.00 eV).⁵⁷ Moreover, the CO molecule is perpendicular to the Ni(100) surface, with the C–O bond length of 1.215 Å and the average Ni–C bond length of 2.042 Å, which are consistent with the reported values of 1.227 and 2.047 Å, for the C–O and Ni–C bond lengths, respectively.⁵⁸

In the case of C and O atoms, no matter where they are placed, they also migrate to the four-fold site after geometry optimization, suggesting that C and O atoms prefer to be adsorbed at the four-fold hollow sites, rather than the top and bridge sites, which is in good agreement with the previous DFT results.^{57,93} The adsorption energies of the C and O atoms are –8.38 and –6.08 eV, respectively, which have the C–Ni bond length of 1.839 Å and the O–Ni bond length of 1.949 Å.

3.1.3 Ni(110) surface. For one CO molecule adsorbed at the five adsorption sites of the Ni(110) surface, CO adsorbed at the short-bridge site is the most stable configuration, with the C–Ni and C–O distances of 1.873 and 1.183 Å, respectively, which are in complete accord with the previous DFT calculated results.⁶⁰ The adsorption energy (–1.83 eV) is similar to the available data obtained by PBE functional (–1.89 eV) in a p(2 × 2) model,⁶⁰ and the PW91 functional (–1.79 eV).⁸⁴ The calculated adsorption energies of CO decrease in the order of pseudo three-fold hollow (–1.71 eV) > four-fold hollow (–1.68 eV) > top (–1.66 eV) > long-bridge (–1.53 eV) sites.

For C atoms, adsorption at the long-bridge site is the most stable configuration, in which the C atom coordinates with two surface Ni atoms and two subsurface Ni atoms; the corresponding adsorption energy is –7.48 eV, with the average C–Ni bond length of 1.835 Å. The O atom prefers to adsorb at the pseudo three-fold hollow site, where it coordinates with two surface Ni atoms and one subsurface Ni atom; the corresponding adsorption energy is –5.99 eV, with the average O–Ni bond length of 1.860 Å.

3.2 CO adsorption at different levels of coverage

In order to probe the effect of surface coverage on CO adsorption, we needed to obtain the most stable co-adsorption configurations of CO molecules at the individual coverage level. The stepwise CO adsorption free energies (ΔE_{ads}) have been defined to determine whether the metal surface

attains adsorption saturation, according to the following equation:

$$\Delta E_{\text{ads}} = E_{\text{CO}_{n+1}/\text{slab}} - (E_{\text{CO}_n/\text{slab}} + E_{\text{CO}}) + \Delta E_{\text{ads}}(\text{correction}) \quad (8)$$

The stepwise CO adsorption free energy correction ΔE_{ads} (correction) refers to the change in Gibbs free energy correction between the adsorbed ($n + 1$)CO systems and the adsorbed n CO systems plus the gaseous isolated species (see the ESI†). With this definition, a positive ΔE_{ads} for $n + 1$ adsorbed CO molecules indicates the adsorption saturation with n CO molecules.

In this coverage regime, we investigated all the possible different adsorption patterns of CO molecules, based on the periodic slab with limited size at individual coverage. To obtain the stable adsorption configurations of CO molecules at different coverage levels, the initial adsorption configurations, where one additional CO molecule was added to the previous most stable adsorption configuration, considering different adsorption possibilities, were calculated. The optimized configuration with the lowest total energy is the most stable co-adsorption configuration at the given coverage. All possible adsorption configurations of CO at different coverage levels have been examined and are presented in the ESI† (see Fig. S2–S4). Fig. 2–4 present the most stable adsorption configurations and the corresponding stepwise adsorption free energies of CO molecules at different coverage levels; the corresponding average lengths of C–O bonds on three Ni surfaces are listed in Table 1. Moreover, the C–O vibrational frequencies of the most stable configurations at a given coverage have been calculated for comparison with the experimentally detected CO stretching frequencies, which are listed in Table 2.

3.2.1 Ni(111) surface. For $n = 1$ –3, all CO molecules are located at the hcp sites with the average C–O bond length of about 1.191 Å. The differences in the stepwise adsorption free energies of these CO molecules indicate that the lateral repulsive interactions between the adsorbed CO molecules are very weak.

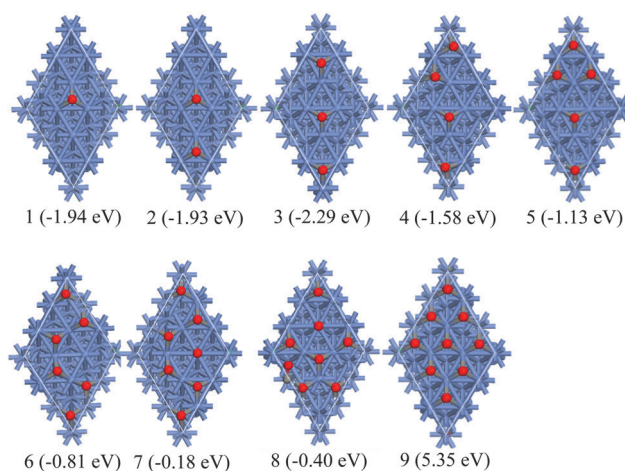


Fig. 2 The most stable configurations and the free energies of the stepwise CO adsorption on Ni(111) surface at different coverage levels.

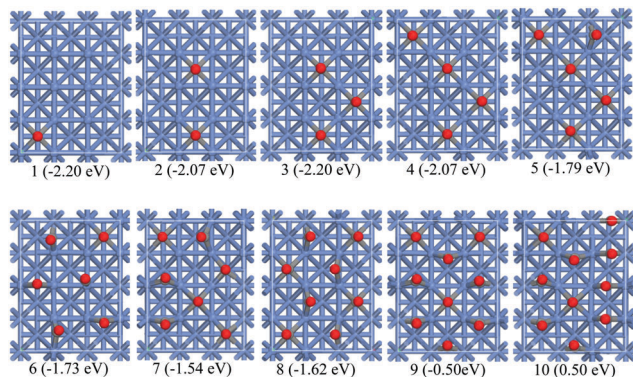


Fig. 3 The most stable configurations and the free energies of the stepwise CO adsorption on the Ni(100) surface at different coverage levels.

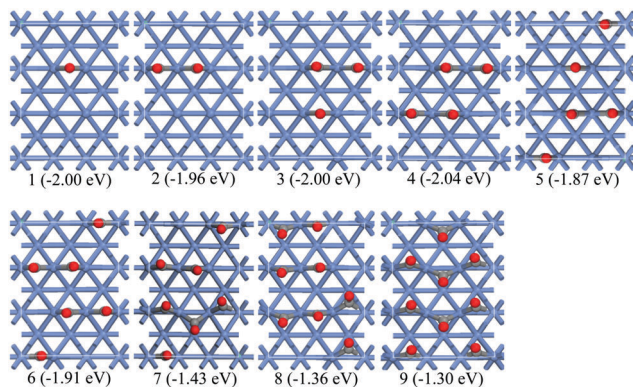


Fig. 4 The most stable configurations and the free energies of the stepwise CO adsorption on the Ni(110) surface at different coverage levels.

Table 1 The average lengths of the C–O bond ($d_{\text{C-O}}/\text{\AA}$) for CO adsorption at different coverage levels on Ni surfaces

	Coverage (ML)								
Surfaces	1/9	2/9	3/9	4/9	5/9	6/9	7/9	8/9	9/9
(111)	1.195	1.193	1.191	1.188	1.183	1.180	1.176	1.172	—
(110)	1.183	1.180	1.179	1.178	1.177	1.176	1.176	1.175	1.179

	Coverage (ML)								
Surfaces	1/12	2/12	3/12	4/12	5/12	6/12	7/12	8/12	9/12
(100)	1.215	1.215	1.227	1.210	1.202	1.181	1.190	1.188	1.180

For $n = 4-6$, all CO molecules are located at the hcp and fcc sites, similar to the findings at the coverage of 0.50 ML.^{27,29-32} Compared to the first three adsorbed CO molecules, the less negative stepwise adsorption free energies and the shorter average C–O bond lengths suggest that the repulsion between CO molecules have begun to affect the stability of CO adsorption.

For $n = 7$, interestingly, one CO molecule stands uprightly at the top site surrounded by six CO molecules adsorbed at the three-fold hollow sites, which maximizes the intermolecular distances, and lowers the Gibbs free energy. However, the weaker stepwise adsorption free energy and the average C–O

Table 2 The calculated and experimental vibrational frequencies ($\nu_{\text{CO}}/\text{cm}^{-1}$) of the C–O bond for CO adsorption at different coverage levels on Ni surfaces

Coverage (ML)	Our calculated values	Experimental values
(111) surface		
1/9	1763	1817, 2045 ²¹
2/9	1760–1786	
3/9	1771–1806	
4/9	1786–1849	
5/9	1786–1897	1815–1910 ^{21,94,95}
6/9	1750–1922	
7/9	1745–1909, 2076	
8/9	1820–1912, 2053–2080	
(100) surface		
1/12	1623	
2/12	1625–1634	1885–1924 ³⁵
3/12	1634–1658	
4/12	1638–1673	2016–2048 ³⁵
5/12	1649–1682, 1876	
6/12	1645, 1847–1893, 2007	1863–1875 ³⁷
7/12	1662–1727, 1860–1897	
8/12	1596–1701, 1886–1934	2019–2029 ³⁷
9/12	1701–1731, 1880–1953	
(110) surface		
1/9	1843	1985 ⁴⁴
2/9	1843–1885	
3/9	1845–1891	
4/9	1848–1905	1880–1940, 1998 ⁴⁵
5/9	1852–1912	
6/9	1855–1924	
7/9	1826–1934	
8/9	1855–1952	1840–1920, 1960 ⁴⁶
9/9	1871–1963	

bond length of 1.176 Å indicate the near saturation coverage of CO adsorption over the Ni(111) surface.

At the coverage level of 8/9 ML, which exceeds the experimental prediction of 0.62 ML at 220 K in an ultrahigh vacuum system, it is no longer energetically favorable to add more CO molecules onto the surface.²⁸ The stepwise adsorption free energy is -0.40 eV, and the average C–O bond length decreased to 1.172 Å, moreover, one CO molecule is far away from the surface due to the strong repulsive lateral interaction. Throughout the adsorption process, it was concluded that CO prevalingly adsorbs at the three-fold hollow site from low to saturated coverage on the Ni(111) surface.

On the other hand, to better understand the adsorptive characterization of CO on the Ni(111) surface, the vibrational frequencies of adsorbed CO molecules at different coverage levels were calculated on the basis of the most stable adsorption configurations. For $n\text{CO} = 1-6$, the C–O bonds of the adsorbed CO molecules have vibrational frequencies in the range of 1750–1922 cm^{-1} , since all CO molecules are adsorbed at the three-fold hollow sites. At the coverage levels of 7/9 and 8/9 ML, there are two types of CO adsorption configurations: the vibrational frequencies in the range of 2053–2080 cm^{-1} at the top sites, and those in the ranges of 1745–1909 and 1820–1912 cm^{-1} at the three-fold hollow sites. The shift of CO vibrational frequencies to higher wave numbers from the low to high coverage exhibits that the C–O bond length is shortened, and the Ni–CO interaction is weakened.

Previous IRAS experimental studies reported by Greenler *et al.* on the Ni(111) surface²¹ have shown that the stretching frequencies of CO adsorbed at the three-fold sites and at the top sites are 1817 and 2045 cm^{-1} , respectively. Moreover, the CO stretching vibrational frequency shifted continuously from about 1815 cm^{-1} at very low coverage, to about 1910 cm^{-1} at the coverage of 0.50 ML on the Ni(111) surface.^{21,94,95} Therefore, the calculated vibrational frequencies in our study are in good agreement with the experimental results, indicating that the most stable configurations of CO adsorption at different coverage levels can be used to understand the effect of coverage on CO adsorption.

3.2.2 Ni(100) surface. For $n = 1-4$, the CO molecules are perpendicularly adsorbed at the four-fold hollow sites on the Ni(100) surface. Compared to the free CO molecules (1.144 Å), the bond lengths (about 1.215 Å) of the adsorbed CO molecules show that the CO molecules become activated at the low coverage levels. The similar stepwise adsorption free energies indicate the weak lateral repulsive interactions between the adsorbed CO molecules.

For $n = 5$, one CO molecule adsorbs at the bridge site, while the others are still located at the four-fold hollow site, which has the stepwise adsorption free energy of -1.79 eV, with the average C–O bond length of 1.202 Å. However, when the coverage increased to 8/12 ML, more CO molecules began to move to the bridge and top sites, in which different tilt degrees of CO molecules appeared among the adsorbed CO molecules to minimize the increasing lateral repulsions. By comparing the stepwise adsorption free energies and the C–O bond lengths at the coverage of $n = 5-8$, with those at the coverage of $n = 1-4$, it was found that the adsorption strength became weaker at high coverage.

At the saturated coverage of 9/12 ML, the average C–O bond length for nine molecules was reduced to 1.180 Å, the stepwise adsorption value increased to -0.50 eV, three CO molecules were adsorbed at the four-fold hollow sites, and six CO molecules were located at the bridge sites.

Throughout the adsorption process on the Ni(100) surface, three adsorption sites (top, bridge and four-fold hollow site) appeared; the bridge and four-fold hollow sites were the dominant adsorption sites. However, no available experimental data at the four-fold hollow sites can be compared with our calculated results since almost all experimental methods could detect only the bridge-bonded and top-bonded CO species,³⁷⁻³⁹ which may be due to the fast dissociation of CO molecules at the four-fold hollow site, leading to rapid build-up of deposited carbon.³⁸ As a result, the carbon species might hinder CO molecules from locating at the four-fold hollow site.

On the Ni(100) surface, CO molecules adsorbed at the four-fold hollow sites have low vibrational frequencies in the range of 1623–1673 cm^{-1} for $n = 1-4$. At the coverage of 5/12 ML, the bridge-bonded CO molecule has the vibrational frequencies of 1876 cm^{-1} , while the others at the four-fold hollow site have the C–O vibrational frequencies in the range of 1649–1682 cm^{-1} . At the coverage of 6/12 ML, there are three adsorption configurations, and the CO vibrational frequencies are 2007 cm^{-1} for

the top configuration, 1847–1893 cm^{-1} for the bridge configuration, and 1645 cm^{-1} for the four-fold hollow configuration. For $n = 7-9$, the calculated CO vibrational frequencies show 1596–1731 cm^{-1} for the four-fold sites and 1860–1953 cm^{-1} for the bridge sites. Experimentally, the FIIRA spectra exhibit the C–O stretching frequencies of 2016–2048 cm^{-1} at the top sites and 1885–1924 cm^{-1} at the bridge sites.³⁵ IRAS also assigned the bands observed at about 2019–2029 cm^{-1} and 1863–1875 cm^{-1} to CO stretching vibrational modes at the top and bridge sites, respectively.³⁷ Therefore, our calculated vibrational frequencies agree well with the experimental observations on the Ni(100) surface.

3.2.3 Ni(110) surface. On the Ni(110) surface, all CO molecules are located at the short-bridge sites, and the C–O bond lengths are elongated to around 1.180 Å at all coverage levels. From $n = 1$ to 6, the stepwise adsorption free energies remain almost constant at about -1.96 eV. At higher coverage, the stepwise adsorption free energies increased to around -1.30 eV, and the slightly tilted CO molecules reduced the repulsive lateral interactions, which is in agreement with the experimental observations that the CO molecules were tilted by about 19° , from ESDIAD measurements, when the coverage was above 0.75 ML.⁹⁶

In general, the stable adsorption site for the CO molecule is the short-bridge site, and the stepwise adsorption free energies slightly change at different coverage levels on the Ni(110) surface, which agree well with the experimental facts that the desorption energy remains almost constant over the whole coverage range on the Ni(110) surface.^{59,97} Further, the saturation coverage of 9/9 ML is also in accordance with the conclusion obtained by Behm *et al.*,⁹⁷ in which the saturation coverage of CO adsorption is also 1.00 ML at temperatures below 250 K.

On the other hand, the calculated vibrational frequency range of 1826–1952 cm^{-1} at the short-bridge site below the coverage of 8/9 ML, is close to the vibrational frequency ranges of 1880–1940 cm^{-1} , below $\theta \approx 0.80$ ML,⁴⁵ and 1840–1920 cm^{-1} below $\theta \approx 0.85$ ML,⁴⁶ for CO adsorption at the bridge sites on the Ni(110) surface. The vibrational frequencies at 1985 cm^{-1} ,⁴⁴ 1998 cm^{-1} ⁴⁵ and 1960 cm^{-1} ⁴⁶ at full monolayer coverage are in general accordance with our frequency ranges from 1871 to 1963 cm^{-1} .

3.3 The lateral repulsive interaction at different coverage levels

In surface science, the intermolecular CO–CO repulsive interaction over metal surfaces, caused by electron transfer between metal and CO species, plays a key role in the adsorption and activation process of CO over the metal surface at different coverage levels. Feng *et al.*,⁹⁸ using scanning tunneling microscopy (STM) and photoelectron spectroscopy at room temperature, observed that the Pt (557) and Pt (332) surfaces break up into nanometer-sized clusters when CO coverage reaches 1.00 ML, which is explained by the strong intermolecular CO–CO repulsion interaction, using DFT calculations. Therefore, the lateral repulsive interaction has an important contribution to the system energy. According to eqn (9),⁹⁹ the lateral interaction can be calculated between the co-adsorption system and the individually adsorbed system.

$$E_{\text{late}} = G_{\text{AB/slab}} + E_{\text{slab}} - G_{\text{A/slab}} - G_{\text{B/slab}} \quad (9)$$

where E_{late} is the lateral interaction, $G_{\text{AB/slab}}$, $G_{\text{A/slab}}$ and $G_{\text{B/slab}}$ are the Gibbs free energies of the co-adsorption AB system, as well as the individual adsorbed A and B systems, respectively.

For describing the CO–CO repulsive interaction on the metal surface, we define the lateral repulsive energy using eqn (10):

$$\Delta E_{\text{late}} = G_{\text{CO}(n+1)/\text{slab}} + E_{\text{slab}} - G_{\text{CO}(n)/\text{slab}} - G_{\text{CO}/\text{slab}} \quad (10)$$

where ΔE_{late} represents the lateral repulsive energy between an added CO molecule and the previous most stable adsorption configuration of CO molecules, $E_{\text{CO}(n+1)/\text{slab}}$ denotes the Gibbs free energy of the system consisting of $(n+1)$ CO molecules and the slab surface, E_{slab} represents the total energy of the pure slab surface, $G_{\text{CO}(n)/\text{slab}}$ and $G_{\text{CO}/\text{slab}}$ are the Gibbs free energy of the slab surface with adsorbed n CO molecules and the slab surface with the single CO molecule, respectively.

Eqn (10) can be further simplified to the difference of a single CO adsorption free energy, $\Delta E_{\text{ads}}(n = 1\text{CO})$, and the stepwise adsorption free energy ΔE_{ads} , as shown in eqn (11):

$$\Delta E_{\text{late}} = \Delta E_{\text{ads}} - \Delta E_{\text{ads}}(n = 1\text{CO}) \quad (11)$$

The corresponding lateral repulsive energies of CO molecules on the three Ni surfaces at different coverage levels are shown in Table 3. On the (111) surface, the lateral interaction energies at the coverage below 3/9 ML are 0.02 and -0.34 eV, respectively. When the shared surface Ni atoms appear at the coverage levels of $n = 4$ and 5, the CO molecules have repulsion interactions with each other. Correspondingly, the repulsive energies increase sharply to 0.36 and 0.82 eV, respectively. For $n = 6$ and 7, the crowded CO molecules over the Ni surface lead to the greater repulsive interactions of 1.14 and 1.77 eV, respectively, and the strong lateral repulsive interaction explains the above-mentioned characteristic structure at the coverage of $n = 7$, in which one CO molecule is adsorbed in an upright position at the top site, surrounded by other CO molecules located at the three-fold hollow sites. The lateral repulsive energy (1.54 eV) at the saturation coverage of 8/9 ML causes the CO molecule to ultimately stay far away from the surface.

A similar phenomenon also occurs on the Ni(100) surface, where the lateral repulsive interactions increase with the increasing coverage. When the amount of CO molecules increases to 7 and 8, they migrate alternately from the four-fold hollow site to

the bridge site, so as to adjust the distances between themselves and their partners. However, at the saturated coverage of 9/12 ML, since CO molecules cannot adjust the distances between themselves and their partners within the limited Ni(100) surface areas, two-thirds of the CO molecules move to the bridge sites, leading to the repulsive interactions of 1.69 eV.

Interestingly, unlike the flat Ni(111) and (100) surfaces, for the corrugated Ni(110) surface, when the coverage is below 6/9 ML, the lateral interactions are ≤ 0.13 eV. Although the lateral repulsive interactions increase to 0.57 and 0.64 eV at the coverage of 7/9 and 8/9 ML, respectively, they are still weaker than those on the flat (111) and (100) surfaces at the same coverage; only the repulsive interaction of 0.69 eV is found at the saturation coverage, due to the tilting of the CO molecules. Therefore, for the Ni(110) surface, we can conclude that both the corrugated surface with the large surface area and the tilting of CO molecules dominantly contribute to the weakness of the lateral repulsive interactions between CO molecules.

Overall, with the increasing CO coverage on the flat Ni(111) and (100) surfaces, the strong lateral repulsive interaction and substrate-mediated metal-sharing effects tend to dominate the stability of the CO molecules on the metal surface, and alter their preferable adsorption configurations. However, on the corrugated (110) surface, the lateral repulsive interaction of CO molecules is independent of coverage, due to the larger CO intermolecular distances. Moreover, the lateral repulsive interaction on the flat surface is stronger than that on the corrugated surface.

3.4 CO dissociation and desorption at different coverage levels

As mentioned above, the saturation coverage of CO molecules (the most stable adsorption configuration) and its stepwise adsorption free energy at different coverage levels have been obtained on three Ni surfaces. In order to probe the adsorption state of the CO molecules at different coverage levels, we made a comparison between the dissociation and desorption of CO adsorbed on these surfaces. In the CO dissociative reaction, the free energy barrier of CO dissociation (E_{a}) and the reaction free energy (ΔE_{dis}) are defined as follows:

$$E_{\text{a}} = E_{\text{TS}} - E_{\text{IS}} + \Delta E_{\text{a}} \text{ (correction)} \quad (12)$$

$$\Delta E_{\text{dis}} = E_{\text{FS}} - E_{\text{IS}} + \Delta E_{\text{dis}} \text{ (correction)} \quad (13)$$

where E_{IS} , E_{FS} , and E_{TS} are the total energies of the surface with the initially adsorbed CO molecule, the final dissociated C and O atoms, and the transition states of this reaction, respectively; the dissociation free energy barrier correction ΔE_{a} (correction) refers to the change in Gibbs free energy correction between transition states and initial states; the dissociation reaction free energy correction ΔE_{dis} (correction) corresponds to the change in Gibbs free energy correction between final states and initial states (see the ESI[†]). The corrected stepwise adsorption free energies further serve as the reverse stepwise desorption free energies, to carry out a comparison between the dissociation and desorption of adsorbed CO molecules over Ni surfaces.

Table 3 The lateral repulsive energies (ΔE_{late} /eV) between an added CO and the previous most stable adsorption configuration of CO molecules at different coverage levels on Ni surfaces

	Coverage (ML)								
Surfaces	1/9	2/9	3/9	4/9	5/9	6/9	7/9	8/9	9/9
(111)	0.00	0.02	-0.34	0.36	0.82	1.14	1.77	1.54	—
(110)	0.00	0.04	0.00	-0.04	0.13	0.09	0.57	0.64	0.69
	Coverage (ML)								
Surfaces	1/12	2/12	3/12	4/12	5/12	6/12	7/12	8/12	9/12
(100)	0.00	0.13	0.00	0.13	0.40	0.47	0.65	0.58	1.69

Table 4 The C–O bond distances in the transition state (Å), CO stepwise desorption free energies ($\Delta E_{\text{des}}/\text{eV}$), dissociation free energy barriers (E_{a}/eV) and reaction free energies ($\Delta E_{\text{dis}}/\text{eV}$), including the zero-point energy correction, thermal energy correction, entropies at the temperature of 523 K, and the corresponding dissociation ($r_{\text{dis}}/\text{s}^{-1} \text{ site}^{-1}$) and desorption ($r_{\text{des}}/\text{s}^{-1} \text{ site}^{-1}$) rates at different coverage levels on Ni surfaces

Coverage (ML)	Dissociation pathways	$d_{\text{C-O}}$	E_{a}	ΔE_{des}	ΔE_{dis}	r_{dis}	r_{des}
(111) surface							
1/9	1CO \rightarrow 1C + 1O	1.865	3.72	1.94	1.52	1.52×10^{-24}	2.43×10^{-7}
2/9	2CO \rightarrow 1CO + 1C + 1O	1.876	3.75	1.93	1.53	1.37×10^{-24}	9.13×10^{-7}
	1CO + C + O \rightarrow 2C + 2O	—	—	1.76	—	—	—
3/9	3CO \rightarrow 2CO + 1C + 1O	—	—	2.29	—	—	—
(100) surface							
1/12	1CO \rightarrow 1C + 1O	1.917	1.90	2.20	0.12	3.84×10^{-7}	5.93×10^{-10}
2/12	2CO \rightarrow 1CO + 1C + 1O	1.909	1.95	2.07	0.04	2.35×10^{-7}	1.53×10^{-8}
	1CO + C + O \rightarrow 2C + 2O	1.919	2.02	1.80	0.20	2.13×10^{-8}	4.49×10^{-6}
3/12	3CO \rightarrow 2CO + 1C + 1O	1.908	1.92	2.20	0.18	6.41×10^{-7}	2.14×10^{-9}
	2CO + 1C + 1O \rightarrow 1CO + 2C + 2O	1.896	2.00	1.71	0.20	6.44×10^{-8}	6.02×10^{-5}
	1CO + 2C + 2O \rightarrow 3C + 3O	2.020	2.80	1.72	1.71	5.50×10^{-16}	2.41×10^{-5}
4/12	4CO \rightarrow 3CO + 1C + 1O	1.917	2.25	1.66	0.38	5.02×10^{-10}	3.67×10^{-4}
5/12	5CO \rightarrow 4CO + 1C + 1O	1.921	2.06	1.79	0.36	3.72×10^{-8}	2.55×10^{-5}
(110) surface							
1/9	1CO \rightarrow 1C + 1O	1.942	1.96	2.00	0.63	1.39×10^{-7}	6.43×10^{-8}
2/9	2CO \rightarrow 1CO + 1C + 1O	1.997	2.11	1.96	0.96	8.73×10^{-9}	3.13×10^{-7}
	1CO + C + O \rightarrow 2C + 2O	1.993	2.16	1.33	0.83	1.23×10^{-9}	0.18
3/9	3CO \rightarrow 2CO + 1C + 1O	1.996	2.15	2.00	0.92	4.62×10^{-9}	1.93×10^{-7}

Table 4 lists the calculated dissociation free energy barriers, reaction free energy, the stepwise desorption free energies and the corresponding rates at different coverage levels on three Ni surfaces. The corresponding structures of initial states (IS), transition states (TS), and final states (FS) are given in the ESI† (see Fig. S5–S7).

3.4.1 Ni(111) surface. For the dissociation of one CO molecule on the surface, starting from CO adsorbed at the hcp site, CO dissociates into C and O atoms *via* the transition state, TS1, in which the O atom arrives at the top site. In the final state, the dissociated C and O atoms are adsorbed at the hcp and its *para*-fcc sites, respectively. The length of the C–O bond in TS1 is elongated to 1.865 Å. The dissociative reaction is endothermic by 1.94 eV, with the dissociation free energy barrier of 3.72 eV, which agrees well with the available result of 3.74 eV at the low coverage (1/9 ML), as reported by Zhang *et al.*⁵⁴ The dissociation rate is about seventeen orders of magnitude lower, and the free energy barrier is 1.78 eV higher than the desorption energy, suggesting that CO dissociation at the coverage of 1/9 ML is kinetically and thermodynamically unfavorable.

Similar to the coverage of 1/9 ML, the dissociation free energy barrier (3.75 eV) of the first CO molecule at the coverage of 2/9 ML is higher than the desorption free energy (1.93 eV); accordingly, the dissociation rate ($1.37 \times 10^{-24} \text{ s}^{-1} \text{ site}^{-1}$) is lower than the desorption rate ($9.13 \times 10^{-7} \text{ s}^{-1} \text{ site}^{-1}$), suggesting that CO dissociation at the coverage of 2/9 ML is kinetically unfavorable, compared to its desorption. Meanwhile, our results show that when two C and two O atoms are initially adsorbed at the two hcp and two fcc sites, respectively, one C atom can interact with the adjacent O atom to form a CO molecule after geometry optimization, due to the limited O adsorption sites over the Ni(111) surface, there is no opportunity for the dissociation of the second CO molecule.

Surprisingly, for three co-adsorbed CO molecules (3/9 ML), the first CO molecule dissociates into C and O atoms, as well as the other two CO molecules. Our results show that when the C and O atoms, as well as the two CO molecules are initially adsorbed over the surface, one CO molecule can interact easily with the adjacent O atom to form a CO₂ molecule after geometry optimization, which means that CO dissociation cannot occur on the Ni(111) surface at the coverage of 3/9 ML.

The great gap of both the free energy barrier and reaction rate between dissociation and desorption shows that CO dissociation into C and O atoms is unfavorable, compared to its desorption at the lowest coverage (1/9 ML); moreover, since there are unavailable adsorption sites at coverage $\geq 2/9$ ML, CO molecules cannot dissociate into atomic C and O. Therefore, CO will adsorb molecularly on the Ni(111) surface in the methanation process.

3.4.2 Ni(100) surface. For the single CO dissociation on the surface, CO dissociates *via* the transition state, TS1, into C and O atoms, which are located at two adjacent four-fold hollow sites. In TS1, the C–O bond length is elongated to 1.917 Å. The computed dissociation free energy barrier (1.90 eV) agrees well with the result of 1.87 eV at low coverage, reported by Andersson *et al.*³⁴ The dissociation free energy barrier is lower than the desorption energy (2.20 eV); correspondingly, the dissociation rate of $3.84 \times 10^{-7} \text{ s}^{-1} \text{ site}^{-1}$ is higher than the desorption rate of $5.93 \times 10^{-10} \text{ s}^{-1} \text{ site}^{-1}$. Thus, CO dissociation is more favorable than desorption at the coverage of 1/12 ML.

For two co-adsorbed CO molecules (2/12 ML), they will dissociate into CO + C + O, followed by further dissociation into the final 2C + 2O state on the surface. The stepwise dissociation free energy barriers of 1.95 eV for the first CO and 2.02 eV for the second CO, are lower than their corresponding desorption free energies (2.07 and 1.80 eV), suggesting that there will be dissociative and molecular adsorption of CO molecules at this coverage under realistic conditions.

When the coverage is up to 3/12 ML, the dissociation free energy barrier of the first CO molecules (1.92 eV) is lower than the corresponding desorption free energy (2.20 eV). However, the dissociation barriers of the second and third CO molecule (2.00 and 2.80 eV) become much higher than their desorption free energies (1.71 and 1.72 eV). Thus, these CO molecules can have equilibrium between dissociation and desorption at the coverage of 3/12 ML. Furthermore, with the increase of the dissociation numbers of CO molecules at the coverage level, shown in Table 4, the dissociation rate decreased by nine orders of magnitude, and the desorption rate increased by four orders of magnitude, suggesting that the CO dissociation became more difficult, compared with desorption.

At the coverage of 4/12–5/12 ML, the dissociation free energy barriers (2.25 and 2.06 eV) for the first CO molecule become higher than the corresponding desorption free energies (1.66 and 1.79 eV). Correspondingly, the dissociation rates are lower than the desorption rates. As a result, CO dissociation is unfavorable, compared to desorption at these coverage levels.

Since there are free adsorption sites available at low coverage, the lower dissociation free energy barrier with the higher rate indicates that the dissociation of CO into C and O atoms is the preferred route, rather than its desorption at the lowest coverage (1/12 ML); in the range from 2/12 to 3/12 ML, the equilibrium between the dissociation and desorption over the surface occurs. However, with the increase in coverage ($\geq 4/12$ ML), CO molecules should be the most dominant species rather than C and O atoms over the Ni(100) surface.

3.4.3 Ni(110) surface. For the single CO molecule on the surface, CO adsorbed at the short-bridge site dissociates into C and O atoms located at the long-bridge and pseudo three-fold hollow sites, respectively. In the transition state, the C atom moves to the long-bridge position, and the O atom is adsorbed at the short-bridge site, with the distance between C and O atoms of 1.942 Å. This elementary reaction is endothermic by 0.63 eV, and the dissociation free energy barrier is 1.96 eV, which agrees well with the reported result of 1.83 eV at the low coverage level (1/4 ML), reported by Mohsenzadeh *et al.*⁶⁰ The dissociation free energy barrier is slightly lower than the desorption energy of 2.00 eV, and correspondingly, the dissociation rate of $1.39 \times 10^{-7} \text{ s}^{-1} \text{ site}^{-1}$ is higher than the desorption rate of $6.43 \times 10^{-8} \text{ s}^{-1} \text{ site}^{-1}$, suggesting that the CO dissociation is slightly more favorable than desorption at the lowest coverage.

For the dissociation of two co-adsorbed CO molecules (2/9 ML), the two-step dissociation is endothermic by 0.96 and 0.83 eV, with the corresponding dissociation free energy barriers of 2.11 and 2.16 eV, respectively. The dissociation free energy barrier of the second CO molecule is 0.83 eV higher than the corresponding desorption free energy, which leads to the difference of eight orders of magnitude between the dissociation and desorption rates ($1.23 \times 10^{-9} \text{ vs. } 0.18 \text{ s}^{-1} \text{ site}^{-1}$). These results indicate that the CO dissociation at this coverage is unfavorable, compared to desorption. Furthermore, the dissociation of the first CO molecule is still unfavorable, based on the comparison of the free energy barrier and the rates of

dissociation and desorption at the coverage levels of 3/9 ML (2.15 vs. 2.00 eV, and $4.62 \times 10^{-9} \text{ vs. } 1.93 \times 10^{-7} \text{ s}^{-1} \text{ site}^{-1}$).

Consequently, the increasing lateral repulsive interactions make CO dissociation into C and O atoms more difficult at the higher coverage. Thus, CO desorption will compete with dissociation only at the lowest coverage, 1/9 ML, while CO desorption is favored with increasing coverage on the (110) surface.

3.5 General discussion

As mentioned above, the adsorption and dissociation of adsorbed CO molecules at different coverage levels over the three Ni surfaces have been systematically investigated; in this section, we discuss the adsorption state of CO on the Ni surfaces, as well as the effects of the CO coverage, and the surface structure, on the adsorption and dissociation of adsorbed CO molecules.

Compared to the (111) surface, the (100) surface has the lower CO adsorption capacity, with saturation coverage of 9/12 ML, and increasing the coverage leads to the migration of the most stable adsorption sites from the four-fold hollow site to the two-fold bridge site. The Ni(111) surface, which is the most exposed surface of the Ni catalyst, has better CO adsorption capacity with saturation coverage of 8/9 ML. As the coverage increases, the most stable adsorption site converts from the hcp and fcc sites to the top sites in order to balance the lateral interaction of CO molecules. In the process of increasing CO on these two surfaces, both the decrease in the stepwise adsorption free energies and the blue shifts of the CO vibrational frequencies reveal that the CO–Ni interaction is gradually weakened. Therefore, the adsorption sites and adsorption ability of CO molecules over the Ni(111) and (100) surfaces show strong coverage dependence.

Unlike the flat Ni(111) and (100) surfaces, the saturation coverage of CO adsorption over the corrugated (110) surface can reach 1.00 ML, which exhibits the maximum CO adsorption capacity among the three Ni surfaces. All CO molecules prefer to adsorb at the short-bridge site, and the stepwise adsorption free energies and the CO vibrational frequencies remain almost constant at different coverage levels. Therefore, the adsorption sites and adsorption ability of CO over the Ni(110) surface are independent of coverage.

Further, by comparing the stretching vibrational frequencies of CO over the three Ni surfaces on the basis of the most stable adsorption configuration at different coverage levels, the (100) surface has a stronger activation ability toward CO molecules than the (111) and (110) surfaces, from low to high coverage, due to the lower stretching frequencies.

Kinetic analyses were utilized to compare the stepwise CO desorption and dissociation at different coverage levels on the three Ni surfaces, and it was concluded that CO desorption from the (111) surface is more favorable than its dissociation on the surface at all coverage levels. With increasing coverage, there are stronger repulsion interactions, and there are no available adsorption sites for the C and O atoms. A similar case also occurs on the (110) surface, while equilibrium exists between the desorption and dissociation at the lowest coverage; however, on the Ni(100) surface, there are dissociative adsorptions

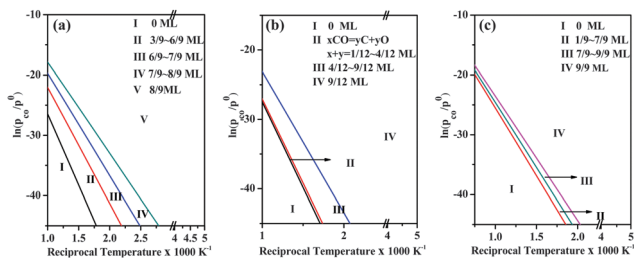


Fig. 5 Equilibrium phase diagram of the stable CO coverage as a function of the temperature and CO partial pressures on different Ni surfaces, (a) Ni(111); (b) Ni(100); (c) Ni(110).

for $n\text{CO} = 1$, and equilibrium exists between molecular and dissociative CO adsorptions for $n\text{CO} = 2-3$. Compared to the (111) and (110) surfaces, the (100) surface has better catalytic ability for CO dissociation.

We further plotted the equilibrium phase diagrams (Fig. 5) of stable CO adsorption states at all possible coverage levels on Ni(111), (100) and (110) surfaces to consider the effects of the different experimental temperatures and CO partial pressures. These phase diagrams not only reveal the change in the stable CO phase coverage with temperature at given pressure, but also provide the saturated stable CO coverage at different T and p_{CO} .

On the most exposed Ni(111) surface, as shown in Fig. 5(a), there are five regions at a given CO partial pressure with increasing temperature: one maximum adsorption region (V, 8/9 ML), and three other CO adsorption regions (IV, 7/9–8/9 ML; III, 6/9–7/9 ML; II, 3/9–6/9 ML), as well as one CO free region (I, 0 ML). Under the ultrahigh vacuum (UHV) conditions (10^{-10} – 10^{-6} Pa, $\ln(p_{\text{CO}}/p^0) = -25.3$ to -34.5), CO molecules adsorbed on the surface start to desorb at 550 K. The desorption temperatures are higher than the experimental TPD results of about 420 K at high coverage on the Ni(111) surface without the support,⁴² but interestingly, they agree very well with the TPD results of CO on Ni/ZrO₂ (SiO₂) ranging from 458 to 762 K.¹⁰⁰ On the Ni(100) surface, as presented in Fig. 5(b), there are four regions: two molecular adsorption regions (IV, 9/12 ML; III, 4/12–9/12 ML), one CO free region (I, 0 ML) and one narrow dissociative adsorption region (II, C + O), which suggests that a fraction of the CO molecules prefer the dissociative adsorption at a given temperature and pressure. Moreover, Ibach *et al.*¹⁰¹ experimentally achieved the CO coverage of 0.80 ML at 300 K by IRAS when the CO pressures increased to 1 mbar (0.150 Pa). Interestingly, our results show that when CO pressures increase to 1 mbar (0.150 Pa), the CO coverage is 0.75 ML at 300 K, which generally agrees with the above experimental facts.¹⁰¹

On the Ni(110) surface, there are four regions, as shown in Fig. 5(c): the broad region (IV) shows the coverage of 9/9 ML, which is quite stable below 813 K, suggesting that the surface is covered with CO molecules under realistic conditions, the other two regions have very narrow temperature ranges (II, 1/9–7/9 ML; III, 7/9–9/9 ML). The last region is the clean surface without CO molecules (I, 0 ML).

On the basis of the above analysis, although the systematic investigations and comparisons reveal that every Ni surface has

characteristic regions at given temperatures and pressures, as well as their difference in CO adsorption states and coverage, it can be qualitatively concluded that molecularly adsorbed CO is the dominant characteristic state at the different temperatures and pressures on Ni surfaces. The computed CO adsorption patterns quantitatively agree with the experiments of the Ni surfaces under ultrahigh vacuum conditions. Consequently, these thermodynamic phase diagrams can still provide useful information for CO adsorption and activation on Ni catalysts, such as the supported Ni catalyst. Therefore, we can apply these phase diagrams to the Ni catalytic system, for example, taking the realistic CO methanation conditions in the range of 423–673 K at atmospheric pressure;¹⁰¹ only molecular adsorption of CO is favorable on the Ni catalyst, which further reveals that direct dissociation of CO is not a major factor for the formation of C on Ni catalysts.

4 Conclusions

In this study, the adsorption and dissociation mechanisms of CO molecules at different coverage levels on three low-index Ni surfaces have been systematically investigated, using dispersion-corrected density functional theory calculations, together with thermodynamic and kinetic analysis at 523 K. The saturated coverage of CO on Ni(111), (100) and (110) surfaces are 8/9, 9/12 and 9/9 ML, respectively. With increasing coverage, the stepwise adsorption free energies become more negative on the flat (111) and (100) surfaces, while little changes occur on the corrugated (110) surface; CO migrates from the three-fold hollow site to the top site on the Ni(111) surface, and from the four-fold hollow site to the two-fold bridge on the (100) surface, while no migration of CO occurs on the (110) surface. Moreover, the computed vibrational frequencies of CO over the three Ni surfaces agree well with the experimental vibrational frequencies, and it can be concluded that the (100) surface has a stronger activation ability toward CO molecules from low to high coverage than the (111) and (110) surfaces. On the other hand, the comparisons based on the kinetic analysis between the stepwise CO desorption and dissociation at different coverage levels on the Ni(111) and (110) surfaces suggest that CO desorption from these surfaces is more favorable than its dissociation at almost all coverage levels. However, on the Ni(100) surface, CO dissociation is more favorable than the desorption at 1/12 ML. When the coverage is 2/12 to 3/12 ML, equilibrium states exist between the dissociation and desorption on the surface. When the coverage is greater than or equal to 4/9 ML, CO desorption becomes more favorable than its dissociation. Compared with the (111) and (110) surfaces, the (100) surface has better ability for CO dissociation.

By the atomistic thermodynamic method, the thermodynamic phase diagrams can provide useful information about CO adsorption and activation on Ni catalysts, including CO adsorption states on each surface, and the equilibrium coverage at a given temperature and pressure. Moreover, a deep understanding of CO adsorption and activation on Ni-based catalysts has been qualitatively achieved, molecular adsorption

is the main characteristic state at different temperatures and pressures on the Ni surface, and further molecular adsorption of CO is favorable on Ni catalyst under realistic methanation conditions.

Acknowledgements

This work is financially supported by the National Natural Science Foundation of China (No. 21276003, 21476155 and 21276171), the Natural Science Foundation of Shanxi Province (No. 2014011012-2), the Program for the Top Young Academic Leaders of Higher Learning Institutions of Shanxi, and the Top Young Innovative Talents of Shanxi.

References

- G. Ertl, H. Knözinger, F. Schüth and J. Weitkamp, *Handbook of Heterogeneous Catalysis*, VCH, Weinheim, 2nd edn, 2008.
- J. M. Thomas and W. J. Thomas, *Principles and Practice of Heterogeneous Catalysis*, Wiley-VCH, Weinheim, 1997.
- M. Ojeda, R. Nabar, A. U. Nilekar, A. Ishikawa, M. Mavrikakis and E. Iglesia, *J. Catal.*, 2010, **272**, 287–297.
- E. D. Park, D. Lee and H. C. Lee, *Catal. Today*, 2009, **139**, 280–290.
- D. W. Jeong, V. Subramanian, J. O. Shim, W. J. Jang, Y. C. Seo, H. S. Roh, J. H. Gu and T. L. Yong, *Catal. Lett.*, 2013, **143**, 438–444.
- D. W. Jeong, H. S. Potdar, K. S. Kim, H. S. Roh and B. Kor, *Chem. Soc.*, 2011, **32**, 3557–3558.
- D. W. Jeong, H. S. Na, J. O. Shim, W. J. Jang, H. S. Roh, U. H. Jung and L. Y. Wang, *Int. J. Hydrogen Energy*, 2014, **39**, 9135–9142.
- S. Shetty and R. A. V. Santen, *Catal. Today*, 2011, **171**, 168–173.
- F. Fischer and H. Tropsh, *Brennst.-Chem.*, 1926, **7**, 97–116.
- R. C. Brady and R. Pettit, *J. Am. Chem. Soc.*, 1980, **102**, 6181–6182.
- B. T. Loveless, B. Corneliu, N. Matthew and I. Enrique, *J. Am. Chem. Soc.*, 2013, **135**, 6107–6121.
- T. Wang, X. X. Tian, Y. W. Li, G. J. Wang, M. Beller and J. H. Jiao, *J. Phys. Chem. C*, 2014, **118**, 3162–3171.
- T. Wang, Y. W. Li, J. G. Wang, M. Beller and H. J. Jiao, *J. Phys. Chem. C*, 2013, **118**, 1095–1101.
- T. Wang, X. X. Tian, Y. W. Li, J. G. Wang, M. Beller and H. J. Jiao, *ACS Catal.*, 2014, **4**, 1991–2005.
- T. Wang, S. G. Wang, Y. W. Li, J. Wang and H. J. Jiao, *J. Phys. Chem. C*, 2012, **116**, 6340–6348.
- F. J. E. Scheijen, D. C. Ferré and J. W. Niemantsverdriet, *J. Phys. Chem. C*, 2009, **113**, 11041–11049.
- Y. S. Tan, Y. Z. Han and S. L. Ma, *J. Nat. Gas Chem.*, 2011, **20**, 435–440.
- J. J. Gao, C. M. Jia, J. Li, F. N. Gu, G. W. Xu, Z. Y. Zhong and F. B. Su, *Ind. Eng. Chem. Res.*, 2012, **51**, 10345–10353.
- A. L. Kustov, A. M. Frey, K. E. Larsen, T. Johannessen, J. K. Nørskov and C. H. Christensen, *Appl. Catal., A*, 2007, **320**, 98–104.
- S. Tada, R. Kikuchi, A. Takagaki, T. Sugawara, S. T. Oyama, K. Urasaki and S. Satokawa, *Appl. Catal., B*, 2013, **140–141**, 258–264.
- J. C. Campuzano and R. G. Greenler, *Surf. Sci.*, 1979, **83**, 301–312.
- L. Surnev, Z. Xu and J. T. Yates, Jr., *Surf. Sci.*, 1988, **201**, 1–13.
- H. Froitzheim and U. Köhler, *Surf. Sci.*, 1987, **188**, 70–86.
- W. Erley, H. Wagner and H. Mach, *Surf. Sci.*, 1979, **80**, 612–619.
- L. Surnev, Z. Xu and J. T. Yates, Jr., *Surf. Sci.*, 1988, **201**, 14–26.
- N. Ikemiya, T. Suzuki and M. Ito, *Surf. Sci.*, 2000, **466**, 119–126.
- P. T. Sprunger, F. Besenbacher and I. Stensgaard, *Chem. Phys. Lett.*, 1995, **243**, 439–444.
- G. Held, J. Schuler, W. Sklarek and H. P. Steinrück, *Surf. Sci.*, 1998, **398**, 154–171.
- R. Davis, D. P. Woodruff, P. Hofmann, O. Schaff, V. Fernandez, K. M. Schindler, V. Fritzsche and A. M. Bradshaw, *J. Phys.: Condens. Matter*, 1996, **8**, 1367–1379.
- L. Becker, S. Aminpirooz, B. Hillert, M. Pedio, J. Haase and D. L. Adams, *Phys. Rev. B: Condens. Matter Mater. Phys.*, 1993, **47**, 9710–9714.
- L. D. Mapledoram, M. P. Bessent, A. Wander and D. A. King, *Chem. Phys. Lett.*, 1994, **228**, 527–532.
- M. E. Davila, M. C. Asensio, D. P. Woodruff, K. M. Schindler, P. Hofmann, K. U. Weiss, R. Dippel, P. Gardner, V. Fritzsche, A. M. Bradshaw, J. C. Conesad and A. R. González-Elipe, *Surf. Sci.*, 1994, **311**, 337–348.
- L. Ng, K. J. Uram, Z. Xu, P. L. Jones and J. T. Yates, *J. Chem. Phys.*, 1987, **86**, 6523–6530.
- M. P. Andersson, F. Abild-Pedersen, I. N. Remediakis, T. Bligaard, G. Jones, J. Engbæk, O. Lytken, S. Horch, J. H. Nielsen and J. Sehested, *J. Catal.*, 2008, **255**, 6–19.
- J. Lauterbach, M. Wittmann and J. Küppers, *Surf. Sci. Lett.*, 1992, **279**, 287–296.
- J. P. Biberian and M. A. V. Hove, *Surf. Sci.*, 1982, **118**, 443–464.
- J. Yoshinobu and M. Kawai, *Surf. Sci.*, 1996, **363**, 105–111.
- G. Rupprechter, T. Dellwig, H. Unterhalt and H. J. Freund, *Top. Catal.*, 2001, **15**, 19–26.
- S. Andersson and J. B. Pendry, *Phys. Rev. Lett.*, 1979, **43**, 363–366.
- C. Zhao and M. A. Passler, *Surf. Sci.*, 1994, **320**, 1–6.
- N. Pangher and J. Haase, *Surf. Sci. Lett.*, 1993, **292**, L908–L911.
- J. C. Bertolini and B. Tardy, *Surf. Sci.*, 1981, **102**, 131–150.
- D. J. Hannaman and M. A. Passler, *Surf. Sci.*, 1988, **203**, 449–462.
- B. J. Bandy, M. A. Chesters, P. Hollins, J. Pritchard and N. Sheppard, *J. Mol. Struct.*, 1982, **80**, 203–208.
- S. Haq, J. G. Love and D. A. King, *Surf. Sci.*, 1992, **275**, 170–184.

- 46 J. Bauhofer, M. Hock and J. Küppers, *Surf. Sci.*, 1987, **191**, 395–405.
- 47 B. Voigtländer, D. Bruchmann, S. Lehwald and H. Ibach, *Surf. Sci.*, 1990, **225**, 151–161.
- 48 O. Knauff, U. Grosche, H. P. Bonzel and V. Fritzsche, *Mol. Phys.*, 1992, **76**, 787–805.
- 49 K. Kośmider, R. Kucharczyk and L. Jurczyszyn, *Appl. Surf. Sci.*, 2013, **267**, 4–7.
- 50 M. Gajdos, A. Eichler and J. Hafner, *J. Phys.: Condens. Matter*, 2004, **16**, 1141–1164.
- 51 F. Abild-Pedersen and M. P. Andersson, *Surf. Sci.*, 2007, **601**, 1747–1753.
- 52 R. C. Catapan, A. A. M. Oliveira, Y. Chen and D. G. Vlachos, *J. Phys. Chem. C*, 2012, **116**, 20281–20291.
- 53 L. Y. Gan, R. Y. Tian, X. B. Yang, H. D. Lu and Y. J. Zhao, *J. Phys. Chem. C*, 2011, **116**, 745–752.
- 54 Q. F. Zhang, B. Han, W. X. Tang, K. Heier, J. X. Li, J. Hoffman, M. Lin, S. L. Britton, A. Derecskei-Kovacs and H. Cheng, *J. Phys. Chem. C*, 2012, **116**, 16522–16531.
- 55 Y. A. Zhu, D. Chen, X. G. Zhou and W. K. Yuan, *Catal. Today*, 2009, **148**, 260–267.
- 56 H. S. Benggaard, J. K. Nørskov, J. Sehested, B. S. Clausen, L. P. Nielsen, A. M. Molenbroek and J. R. Rostrup-Nielsen, *J. Catal.*, 2002, **209**, 365–384.
- 57 B. Hammer and L. B. Hansen, *Phys. Rev. B: Condens. Matter Mater. Phys.*, 1999, **59**, 7413–7421.
- 58 Y. H. Zhou, P. H. Lv and G. C. Wang, *J. Mol. Catal. A: Chem.*, 2006, **258**, 203–215.
- 59 E. Demirci, C. Carbogno, A. Groß and A. Winkler, *Phys. Rev. B: Condens. Matter Mater. Phys.*, 2009, **80**, 1956–1960.
- 60 A. Mohsenzadeh, T. Richards and K. Bolton, *J. Mol. Model.*, 2015, **21**, 1–11.
- 61 G. Kresse and J. Furthmüller, *Phys. Rev. B: Condens. Matter Mater. Phys.*, 1996, **54**, 11169–11186.
- 62 G. Kresse and J. Furthmüller, *Comput. Mater. Sci.*, 1996, **6**, 15–50.
- 63 J. P. Perdew, K. Burke and M. Ernzerhof, *Phys. Rev. Lett.*, 1996, **77**, 3865–3868.
- 64 J. A. White and D. M. Bird, *Phys. Rev. B: Condens. Matter Mater. Phys.*, 1994, **50**, 4954–4957.
- 65 J. Carrasco, L. Barrio, P. Liu, J. A. Rodriguez and M. Veronica Ganduglia-Pirovano, *J. Phys. Chem. C*, 2013, **117**, 8241–8250.
- 66 Z. Y. Wang, X. M. Cao, J. H. Zhu and P. Hu, *J. Catal.*, 2014, **311**, 469–480.
- 67 S. Grimme, *J. Comput. Chem.*, 2004, **25**, 1463–1473.
- 68 S. Grimme, *J. Comput. Chem.*, 2006, **27**, 1787–1799.
- 69 D. C. Sorescu, J. Lee, W. A. Al-Saidi and K. D. Jordan, *J. Chem. Phys.*, 2011, **134**, 104707.
- 70 T. Lu and F. W. Chen, *J. Mol. Model.*, 2013, **19**, 5387–5395.
- 71 G. Kresse and J. Hafner, *Surf. Sci.*, 2000, **459**, 287–302.
- 72 J. P. Clay, J. P. Greeley, F. H. Ribeiro, W. N. Delgass and W. F. Schneider, *J. Catal.*, 2014, **320**, 106–107.
- 73 G. Chiarotti, *Physics of Solid Surfaces*, Springer-Overflag, Berlin, 1995, p. 24.
- 74 C. Kittel, *Introduction to Solid State Physics*, Wiley, 1986.
- 75 Y. H. Zhao, M. M. Yang, D. Sun, H. Y. Su, K. Sun, X. Ma, X. Bao and W. X. Li, *J. Phys. Chem. C*, 2011, **115**, 18247–18256.
- 76 J. A. Dean, *Lange's Handbook of Chemistry*, McGraw-Hill, 15th edn, 1999.
- 77 D. Sheppard, P. Xiao, W. Chemelewski, D. D. Johnson and G. Henkelman, *J. Chem. Phys.*, 2012, **136**, 074103.
- 78 S. Daniel, T. Rye and H. Graeme, *J. Chem. Phys.*, 2008, **128**, 134106.
- 79 G. Henkelman and H. Jónsson, *J. Chem. Phys.*, 1999, **111**, 7010–7022.
- 80 R. A. Olsen, G. J. Kroes, G. Henkelman, A. Arnaldsson and H. Jónsson, *J. Chem. Phys.*, 2004, **121**, 9776–9792.
- 81 L. Joos, I. A. W. Filot, S. Cottenier, E. J. M. Hensen, M. Waroquier, V. V. Speybroeck and R. A. V. Santen, *J. Phys. Chem. C*, 2014, **118**, 5317–5327.
- 82 S. Yamagishi, S. J. Jenkins and D. A. King, *Surf. Sci.*, 2003, **543**, 12–18.
- 83 J. Xu and M. Saeys, *J. Phys. Chem. C*, 2008, **112**, 9679–9685.
- 84 V. Shah, T. Li, H. S. Cheng and K. Baumert, *Fuel Chemistry Division Preprints*, 2002, **47**, 217.
- 85 V. Erik, D. R. Loredana, X. L. Ding, B. Alessandro, S. Letizia, V. Luca, R. Mario, F. Paolo, P. Maria, B. Alfonso and G. Comelli, *J. Am. Chem. Soc.*, 2008, **130**, 11417–11422.
- 86 J. J. Gao, Y. L. Wang, Y. Ping, D. C. Hu, G. W. Xu, F. N. Gu and F. B. Su, *RSC Adv.*, 2012, **2**, 2358–2368.
- 87 J. J. Gao, Q. Liu, F. N. Gu, Z. Y. Zhong and F. B. Su, *RSC Adv.*, 2015, **5**, 22759–22776.
- 88 J. Sehested, S. Dahl, J. Jacobsen and J. R. Rostrup-Nielsen, *J. Phys. Chem. B*, 2005, **109**, 2432–2438.
- 89 X. M. Cao, R. Burch, C. Hardacre and P. Hu, *Catal. Today*, 2011, **165**, 71–79.
- 90 X. M. Cao, R. Burch, C. Hardacre and P. Hu, *J. Phys. Chem. C*, 2011, **115**, 19819–19827.
- 91 D. A. McQuarrie, *Statistical Mechanics*, University Science Books, 2000.
- 92 L. Xu, H. Y. Xiao and X. T. Zu, *Chem. Phys.*, 2006, **323**, 334–340.
- 93 S. G. Wang, D. B. Cao, Y. W. Li, J. G. Wang and H. J. Jiao, *Surf. Sci.*, 2006, **600**, 3226–3234.
- 94 W. Erley, H. Wagner and H. Mach, *Surf. Sci.*, 1979, **80**, 612–619.
- 95 J. G. Chen, W. Erley and H. Ibach, *Surf. Sci.*, 1990, **227**, 79–89.
- 96 M. D. Alvey, M. J. Dresser and J. T. Yates, *Surf. Sci.*, 1986, **165**, 447–465.
- 97 R. J. Behm, G. Ertl and V. Penka, *Surf. Sci.*, 1985, **160**, 387–399.
- 98 T. Feng, D. Sefa, L. W. Wang, L. Zhi, D. R. Butcher, B. Hendrik, S. Miquel and G. A. Somorjai, *Science*, 2010, **327**, 850–853.
- 99 J. Chen and Z. P. Liu, *J. Am. Chem. Soc.*, 2008, **130**, 7929–7937.
- 100 D. C. D. D. Silva, S. Letichevsky, L. E. P. Borges and L. G. Appel, *Int. J. Hydrogen Energy*, 2012, **37**, 8923–8928.
- 101 A. Grossmann, W. Erley and H. Ibach, *Surf. Sci.*, 1995, **330**, 646–650.